Bollettino di Geofisica Teorica ed Applicata Vol. 60, n. 1, pp. 123-136; March 2019
DOI 10.4430/bgta0270

Remote sensing of marine oil spills using Sea-viewing Wide Field-of-View Sensor images

Z. Mihoub[1] and A. Hassini[2]

[1] *LRPI Laboratory, Institute of Health and Industrial Safety, University of Batna-2, Batna, Algeria*
[2] *LISIDD Laboratory, Institute of Maintenance and Industrial Safety, University of Oran-2, Oran, Algeria*

(Received: 27 August 2018; accepted: 2 February 2019)

ABSTRACT The aim of this study is to propose and test a new method for detection of oil spills in the world oceans using Sea-viewing wide Field-of-Wiew Sensor (SeaWiFS) imagery embedded in SeaStar satellite. The colour masking technique is proposed to extract the maximum oil spill pixels from the SeaStar/SeaWiFS satellite images by using fusion by arithmetic combination of the spectral bands method. Each image used is converted from RGB (red, green, blue) to HSI (hue, saturation, intensity) system. The resulting oil slicks are obtained visually in the intensity and saturation images. Then, the values of intensity and saturation are analysed to be potentially applied in other images. In this research, we applied our detecting oil spills algorithm in six different scenes, including different regions of the world oceans, and different dates. Finally, to validate our results, the method has been tested by using the oil spill pixel reference ratio. We found that the method can be used to support the detection of oil slicks, in spite of some limitations.

Key words: ocean pollution, remote sensing, oil spills detection, SeaStar/SeaWiFS images, colorimetric methods.

1. Introduction

Oil slicks on sea surface can have different sources such as man-made slicks from illegal discharges of ships or spills resulting from ship accidents, slicks originated from biological activities such as photo-oxidation processes or by planktons, and geological slicks originated as natural hydrocarbon seeps from a reservoir. Including every kind of slick, 10% of ocean surface is estimated to be covered by slicks (Girard-Ardhuin *et al*., 2005). Natural seepage detection is considered to be one of the significant preliminary works for offshore petroleum exploration. However, it does not explain the whole petroleum system by itself, and it should be combined with regular exploration techniques such as seismic interpretation, sample collection from the sea bottom, and geological survey. The oil slick detection and mapping are becoming one of the standard tools for hydrocarbon exploration activities and have been applied to most of the hydrocarbon basins in the world such as Gulf of Mexico (Friedman *et al*., 2002; Migliaccio *et al*., 2011), Santa Barbara Channel, California (Leifer *et al*., 2006), Australian Shelf (O'Brein *et al*., 2005), and south Caspian Sea (Williams and Lawrence, 2002).

One of the remote sensing sensors used in oil spill detection is synthetic aperture radar (SAR). SAR capabilities are widely well demonstrated (Brekke and Solberg, 2005; Akar *et al*., 2011; Migliaccio *et al*., 2011; Lu *et al*., 2013; Linlin *et al*., 2014; Mihoub and Hassini, 2014). SAR is particularly useful for its all-weather and all-day capability, which is in observing the sea at night and at cloudy weather conditions. SAR measurements allow not only observing sea oil slicks but also discriminating them from a broad class of look-alikes, i.e. those calling for weak-damping properties (Mihoub and Hassini, 2014; Migliaccio *et al*., 2015; Buono *et al*., 2016). SAR data has been subject to many efforts to use mathematical techniques to detect and distinguish oil spills from look-alikes based on external information about weather conditions, differences in shape, and contrast to surroundings (Solberg *et al*., 1999; Gambardella *et al*., 2010; Mihoub and Hassini, 2014). The spatial extent of the 2010 Deepwater Horizon oil slick is large enough to be resolvable by the European Space Agency advanced scatterometer (ASCAT) on meteorological operational satellite (MetOp-A), particularly when processed with resolution-enhancement algorithms. By exploiting the effects of surface oil on the radar backscatter from ocean waves, a coarse mapping (resolution ≈ 5 km) of oil surface extent is made by examining data processed from ASCAT. Although originally designed for only low-resolution ocean wind measurements, ASCAT can be used to map the surface extent of large bodies of oil on the ocean surface (Lindsley and Long, 2012). However, SAR has some limitations: SAR data are expensive, not available daily (long revisit time, several days) and cover small areas (reduced swath, 100-500 km).

Optical sensors also have showed potential in oil spill detection. These optical sensors are characterised by very large swaths, short revisit times, and free of charge (Pisano, 2011). Optical sensors measure the solar irradiance being reflected by the sea and the radiance emitted by the sea surface itself, within the visible, infrared (IR), and microwave spectral windows (Bulgarelli and Djavidnia, 2012; Lu *et al*., 2012; Fingas and Brown, 2014). The radiation that have interacted with, or being emitted from, the sea surface, influenced by the optical processes in the surface layer of water, carries the oceanographic information from the sea to the sensor. Thus, the presence of a floating oil film will modify the radiance leaving the sea surface (water-leaving radiance) (Pisano, 2011). The mechanism of this phenomenon mainly depends on the optical properties of the sea surface and of the oil film (i.e. absorption and scattering coefficients), which in turn depend on sea state (wind and waves) and on the zenith angle of the incident light and of satellite (Taylor, 1992; Fingas and Brown, 1997; Pisano, 2011).

It has been known for some time that oil on the water surface is better viewed with polarised lenses. Several workers have noted the polarising effects of oil on water and have proposed methods to use this phenomenon to distinguish oil (Yuan *et al*., 2010, 2011; Fingas and Brown, 2014). Sun glitter is a particular problem in visible remote sensing. Sun glitter can sometimes be confused for oil sheens. Several workers have found ways to reduce or to deal with sun glitter (Fingas and Brown, 2014).

High resolution optical sensors such as Landsat ETM+, SPOT, IKONOS do not provide daily observations, and the data with limited spatial coverage are expensive. The new optical sensor technologies provide an unprecedented capability for oil spill monitoring in marine environments. Oil spills detection is better achieved by using the Sea-viewing wide Field-of-Wiew Sensor (SeaWiFS) radiometer of the SeaStar satellite because it has wide spectral coverage comprising the visible (ch1, 0.41 μm, to ch6, 0.67 μm), and near-infrared (ch7, 0.76 μm and ch8, 0.86 μm) wavebands. All channels pertain to certain attributes of oil spill, but contain different information.

SeaWiFS measures light intensity in several bands. The measurements allow quantification of

light absorption and subsequent estimation of slicks. SeaWiFS improves by having better bands for atmospheric correction (i.e. removing the effect of light scattering by the Earth's atmosphere), which will particularly aid the estimation of oil slicks places.

In light of their unique and important role in oil spill detection, SeaWiFS images are the focus of this work. This paper presents an idea which derives from the fusion of the satellite images. The images resulting from only one process are not enough with the thematic requests for the diagnosis and the treatment. However, to separately observe a series of multimode images of the same object is not a better solution. The fusion of these data is thus a paramount stage. There are three methods of fusion (Hassini *et al*., 2008):

- statistical methods, like the principal component analysis (PCA) method;
- methods resulting from signal processing, like the wavelet transformer (WT) method;
- colorimetric methods, like the fusion by arithmetic combination (FAC) of spectral bands method.

The FAC method is classified in the colorimetric part, because it is often used with an aim of visual improvement of the data. Of all the methods used, it is the simplest; however, its effectiveness depends on the data input. The images are mixed by addition and/or subtraction and/or product, after D-sampling of the data to the same size. This method is selected in this work.

Each image in this paper is converted from RGB (red, green, and blue) field to HSI (hue, saturation and intensity) field. We seek to obtain the maximum of oil spill pixels on the images; then, one looks at the values taken by intensity and saturation for potentially applying them to other images in routine.

2. Material

2.1. Sensor description

The SeaWiFS on board the SeaStar spacecraft is an advanced sensor designed for ocean monitoring. It consists of eight spectral bands of very narrow wavelength ranges, between 402-885 nm (see Table 1). Applications for imagery include ocean primary production and phytoplankton processes, ocean influences on climate processes (heat storage and aerosol formation), and monitoring of the cycles of carbon, sulfur, and nitrogen. The orbit altitude is 705 km with a local equatorial crossing time of 12 PM. Table 1 is a listing of the central wavelengths and bandwidths for SeaWiFS (Grégoire *et al*., 2002; Hassini *et al*., 2008).

2.2. SeaWiFS level - 1A data

There are Level-1A products for each of the following data types: global-area coverage (GAC), local-area coverage (LAC), lunar calibration, solar calibration, and high resolution picture transmission (HRPT) for direct-readout data (Leblon *et al*., 2007). GAC data are sub sampled from full-resolution data with every fourth pixel of a scan line (from LAC pixels 147 to 1135) and every fourth scan line being recorded for each swath (the Earth data collection portion of an orbit). Thus, GAC data are comprised of 2048 pixels per scan line, whereas all other types are comprised of 1285 pixels per scan line. A GAC scene will also represent an entire swath; whereas LAC scenes are defined by the number of continuously recorded scans, and HRPT scenes are defined by the number of continuously received scans from one satellite pass (Hassini *et al*., 2005).

Table 1 - SeaWiFS sensor description.

Instrument Bands	
Band	Wavelength
1	402-422 nm
2	433-453 nm
3	480-500 nm
4	500-520 nm
5	545-565 nm
6	660-680 nm
7	745-785 nm
8	845-885 nm
Mission Characteristics	
Orbit Type	Sun Synchronous at 705 km
Equator Crossing	Noon +20 min, descending
Orbital Period	99 minutes
Swath Width	2,801 km LAC/HRPT (58.3 degrees)
Swath Width	1,502 km GAC (45 degrees)
Spatial Resolution	1.1 km LAC, 4.5 km GAC
Real-Time Data Rate	665 kbps
Transmission Frequency	1702.5 MHz (encrypted)
Revisit Time	1 day
Digitization	10 bits

2.3. Oil spills detection

This paper presents an idea which derives from the fusion of the satellite images.

SeaStar/SeaWiFS radiometer has two major advantages for oil spills monitoring. First, the instrument provides daily coverage of the entire planet at a moderate spatial resolution (approximately 1 km), which is critical for operational global oil slicks monitoring. Second, it has wide spectral coverage comprising the visible (ch1, 0.41 μm, to ch6, 0.67 μm), and near-infrared (ch7, 0.76 μm and ch8, 0.86 μm) wavebands. All channels pertain to certain attributes of oil slicks, but contain different information (Kaufman and Remer, 1994; Hassini *et al*., 2008). Oil is more discernible in the visible channels, which has been employed to estimate oil spills location. However, the detection of oil slicks is better achieved with RGB and HSI combinations of SeaWiFS channels.

3. Method

3.1. RGB to HSI components conversion

The RGB colour model is an additive colour model in which red, green, and blue light are added together in various ways to reproduce a broad array of colours. The main purpose of the RGB colour model is for the sensing, representation, and display of images in electronic systems,

such as televisions and computers, though it has also been used in conventional photography. Before the electronic age, the RGB colour model already had a solid theory behind it, based in human perception of colours, colour images are always perceived in terms of hue, saturation, and luminance in human visual system.

The HSI format, one of the most widely-used colour coordinate system in colour image processing, was developed by Munsell (1969) and are compatible with the scheme human perceive colour (Munsell, 1969; Uchiyama and Arbib, 1994). It is based on intuitive sensation of colour, and closely simulates the behaviour of human eyes (Horng *et al*., 2005).

The geometric conversion from the familiar RGB colour model to the HSI colour model can be found in Fig. 1. Hue represents a dominant (pure) colour as perceived by an observer. Saturation refers to the amount of white light mixed with a hue.

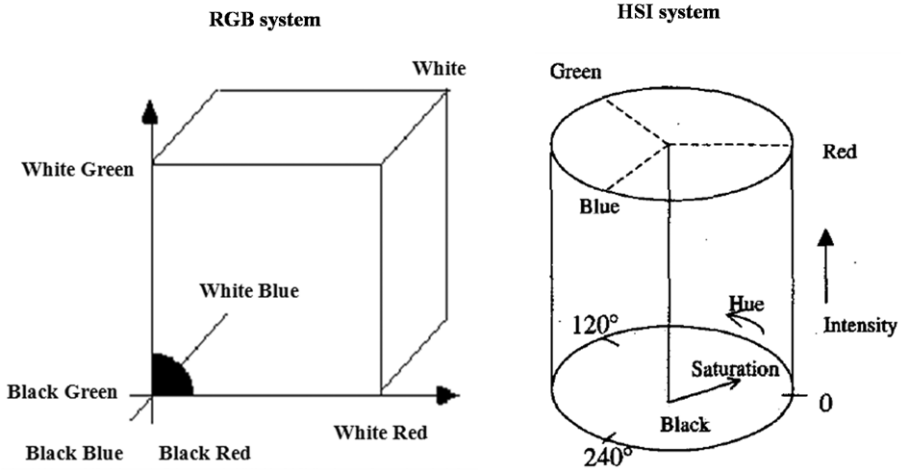

Fig. 1 - Geometric representation of RGB and HSI systems.

Two important facts make the HSI colour model useful to simulate the colour sensing properties of the human visual system. First, the intensity component is decoupled from the colour information in an image. Second, the hue and saturation components are intimately related to the way in which human beings perceive colour. In the following Eqs. 1 to 4, the formulae for conversion are listed for reference (Horng *et al*., 2005; Hassini *et al*., 2008).

$$i = \frac{r+g+b}{3} \tag{1}$$

$$s = 1 - \frac{3}{r+g+b}[\min(r, g, b)] \tag{2}$$

$$h = \begin{cases} \theta & if \quad b \le g \\ 360 - \theta & if \quad b > g \end{cases} \tag{3}$$

where:

$$\theta = \sec\left\{\frac{\frac{1}{2}\left[(r-g)+(r-b)\right]}{\left[(r-g)^2+(r-b)(g-b)\right]^{1/2}}\right\} \tag{4}$$

3.2. Building an oil spill feature model

In the study of image-based oil spill detection, it is necessary to build a more precise oil slicks feature model for vision-based oil spill detection systems. In this research, we used two SeaStar/SeaWiFS images carrying various dates and areas to analyse the colour features of oil spills according to the HSI colour model.

A colour set, C, is a set of colours such that for each colour in the set, represented as a triplet (h, s, i) in the HSI colour model, the following conditions are satisfied: $[s_{min} \le s \le s_{max}]$, and, $[i_{min} \le i \le i_{max}]$ in which $[h_{min}, h_{max}]$ is the range of hue, $[s_{min}, s_{max}]$ is the range of saturation, and $[i_{min}, i_{max}]$ is the range of intensity of the colour set C. Formally, the colour set may be denoted as:

$$C(h,s,i) = \left\{(h,s,i) \,|\, h_{min} \le h \le h_{max}, s_{min} \le s \le s_{max}, i_{min} \le i \le i_{max}\right\} \tag{5}$$

The colour separation algorithm for an input image $f(x, y)$ based on oil spills colour set C is as follows: or each pixel in the image, if the colour of the pixel does belong to the colour set, then set the pixel colour to red; otherwise, keep the pixel colour unchanged (a background colour, unchanged). The result image $g(x, y)$ after performing the above colour separation can be represented as:

$$g(x,y) = \begin{cases} red, & if \quad f(x,y) \in C \\ f(x,y), & otherwise \end{cases} \tag{6}$$

3.3. Hue values in oil spills

Today several techniques for the detection and analysis of oil spilled in water are available: gravimetry, infrared spectrum-photometry, fluorimetry spectra, UV absorption, and surface reflection.

According to colour pixel, the oil slick images belonging to these two classes are fairly different in colour: as regards the first case, pixels appears with a brownish yellow colour, so the dominant colour is brownish, whereas in the second case there are more blueish pixels; colour is between cyan and blue.

Therefore, in several studies, in order to distinguish these two classes, the hue average is adopted as discriminating criterion: images with diluted oil have an average of hue lower than 75, while the images with thick oil passed through by beams have an average of hue greater than 75 (Munsell, 1969). In this study, we assume that the interval of hue values is the same for all images, so the hue value does not affect the results of the applied method.

4. Results and discussions

The form of a Level-1A file name is Syyyydddhhmmss.L1A_ttt, where S is for SeaWiFS, yyyy is the year, ddd is the day of the year (001-366), hh is the hour UTC (00-23), mm is the minute (00-59), and ss is the second (00-59) when the sensor began collecting the scene's data (the first scan line), and ttt is a three- or four-character data type code. In our case, we have used LAC Level 1A images with spatial resolution of 1.1 km at nadir; the form of file name is Syyyydddhhmmss. L1A_MLAC.

Each image product in this paper is generated from a corresponding Level-1A product. The main data contents of the product are the geophysical values for each pixel, derived from the Level-1A raw radiance counts by applying the sensor calibration, and atmospheric corrections.

The radiometric operation of calibration is used to eliminate the side effects on the rough images. They are corrections of the true brightness measured by the radiometer SeaWiFS in order to eliminate the effects of the atmosphere and the solar angle of illumination. Therefore, the effect of incoming solar radiation on the model colorimetric is compensated.

Fig. 2a shows the eight raw channels (6 visible and 2 NIR) of image A (labelled in this work); all channels are splitted and radiometrically calibrated by using ENVI Software (the Environment for Visualizing Images, Research Systems, Inc., Boulder, USA). The file of this image named S2010124202916.L1A_MLAC was received from official source (OCEANCOLOUR GSFC

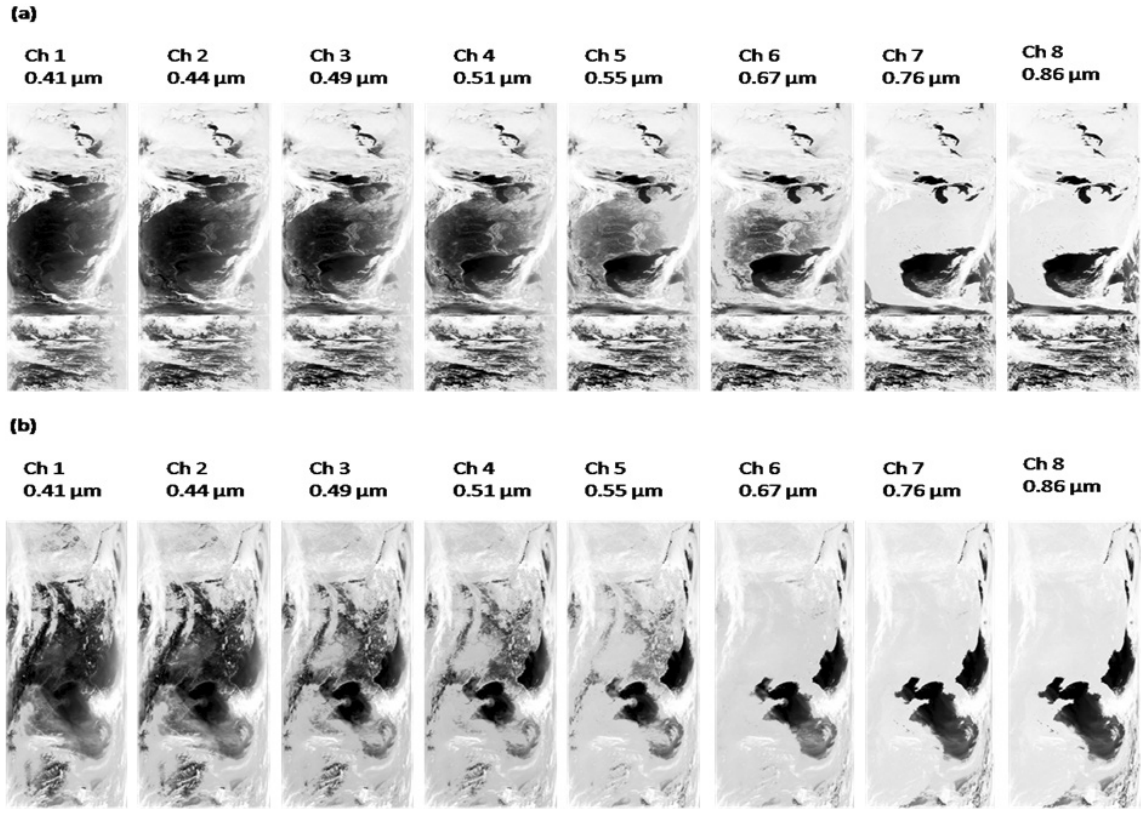

Fig. 2 - Eight spectral channels with the representation of the central spectral wave of each band: a) image A (reference image); b) image B.

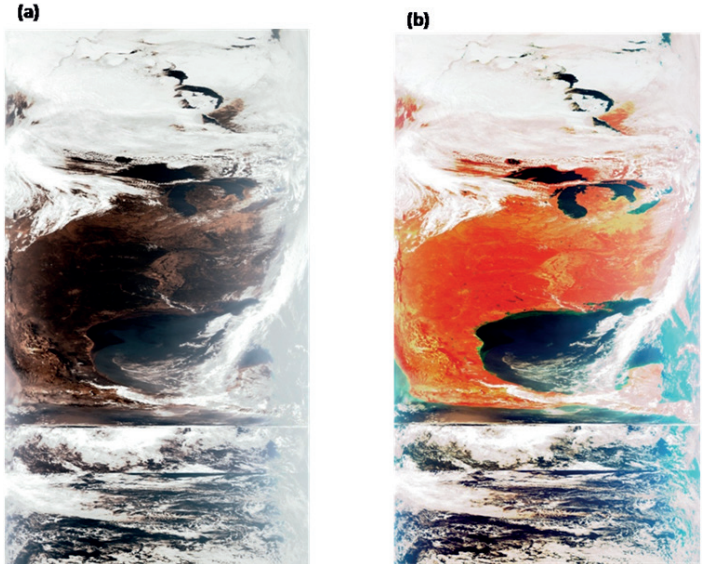

Fig. 3 - Combination result: a) R: ch3, G: ch2, B: ch1; b) R: ch7, G: ch4, B: ch1.

NASA US data base). In this case, our image was received on day 124 (4 May) of year 2010 at 20:29:16 UTC, from level 1A MLAC type.

For each band, the detector measures the intensity of the light that reaches the sensor. When these data are displayed visually, the result is a series of gray-scale images. Notice how different features have different intensities in the various bands. For example, the water appears bright in the blue and purple bands, while land is dark. In the red and infrared bands, it is the land that is bright, while the water is dark. Image A is used to process oil spill pixels covering the Louisiana coast from Deepwater Horizon explosion (2010 Gulf of Mexico oil spill; www.epa.gov/enforcement/deepwater-horizon-bp-gulf-mexico-oil-spill). Because of the important number of oil spill pixels on this image, it is considered like the reference image in this work.

By RGB combination between visible channels 3, 2 and 1 successively (R: ch3, G: ch2, B: ch1) from image A, we can watch clearly the oil slicks along the Louisiana coast (Fig. 3a). This combination most closely represents oil slicks in the visible spectrum. Winds generated large quantities of oil spills, which blanketed the Gulf of Mexico, fortunately there are not clouds, which cover the polluted zone, it is one of the optical data limit. This event can be also clearly watched on the high right part from image of Fig. 3b. This image was realised by combination between the visible and the NIR channels. We have used the following combination R: ch7, G: ch4, B: ch1.

The colour separation algorithm is applied to channel 1, 2 and 3 from image A, by using R: ch3, G: ch2, B: ch1 combination in Eq. 1. The result image is given in Fig. 4. In this image, we can watch the intensity edges of oil slicks presented as red colour separation.

Saturation pixels are calculated by using the same combination (i.e. R: ch3, G: ch2, B: ch1 combination) in Eq. 2, the result is given in Fig. 5. In this image, the region of interest was selected, and the red mask of separation presents the areas of oil slicks.

The other event, on 3 April 2005 incident, which happened near the new port of Dalian in NE China's Liaoning province, oil spills drifts on the water surface in north of the Yellow Sea. This event (image B of Fig. 2b) is acquired by SeaWiFS from the SeaStar satellite.

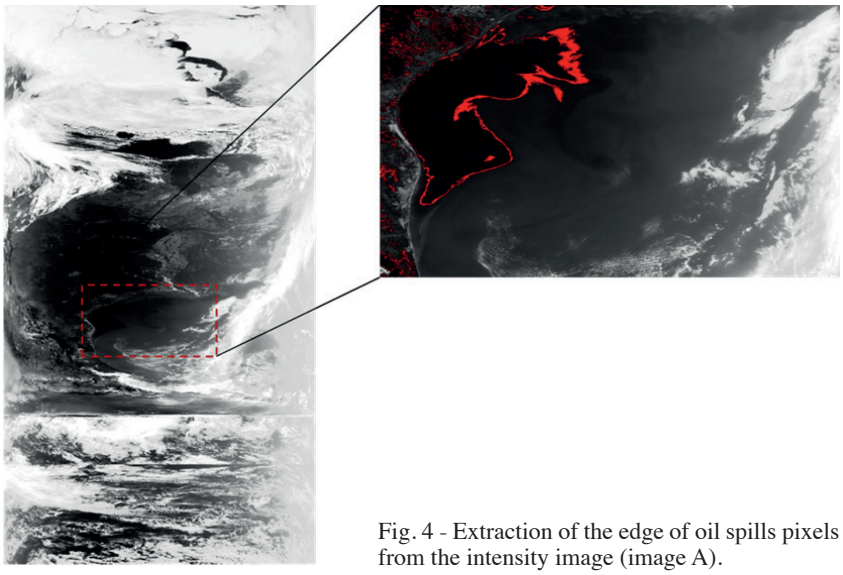

Fig. 4 - Extraction of the edge of oil spills pixels from the intensity image (image A).

Fig. 2b shows the eight spectral channels of the image B (all channels are radiometrically calibrated), whose file is named S2005095041204.L1A_MLAC was acquired on 5 April (095) 2005 and covers the oil spills pixels in the NE China coast. This image is used to validate our research.

The HIS colour model has been adopted because it is intimately related to the way in which human beings perceive colours. According to the empirical analysis of the set of oil spills images, the hue values for oil slicks pixels are: on the one hand, from brownish yellow colour are usually in the range of [0°-60°], on the other hand, from blueish pixels; colour is between cyan and blue, the hue values are in the range [180°-240°]. In this study, we suppose that the hue values are the same for all images; in the range [0°-60°]. So, the hue value does not affect the results of the applied method.

The intensity values in image A are in the range [303, 975] and, on the other hand, the intensity values in image B are in the range [462, 956]. The saturation values after normalisation are distributed in the range [0, 100] in the two images. By using colour separation algorithm (Eq. 6) in image A, the saturation values from the oil spills pixels are in the range [45, 60], and the intensity values from the oil spills pixels are in the range [407, 424].

By using the same RGB combination and the same intervals of the oil spills extracted from image A and Eqs. 1, 2, and 6 (saturation: 407-424, intensity: 45-60, hue: 0°-60°), the active oil spills locations in image B have been enhanced and edged in red colour. In Figs. 6 and 7, we can watch respectively, the intensity edges and saturation pixels of oil spills presented as red colour separation.

The proposed oil spill detection method is tested with five other scenes of images (image C to image F in Table 2) for a variety of conditions, including different regions of the world oceans and different times. The limit values for the oil slicks with HSI system are summarised and the experimental results of the proposed method are shown in Table 3.

Oil spill pixel reference ratio (OSPRR) denotes the detection rate between each image from Table 2 and the reference image (image A). It is defined as the ratio:

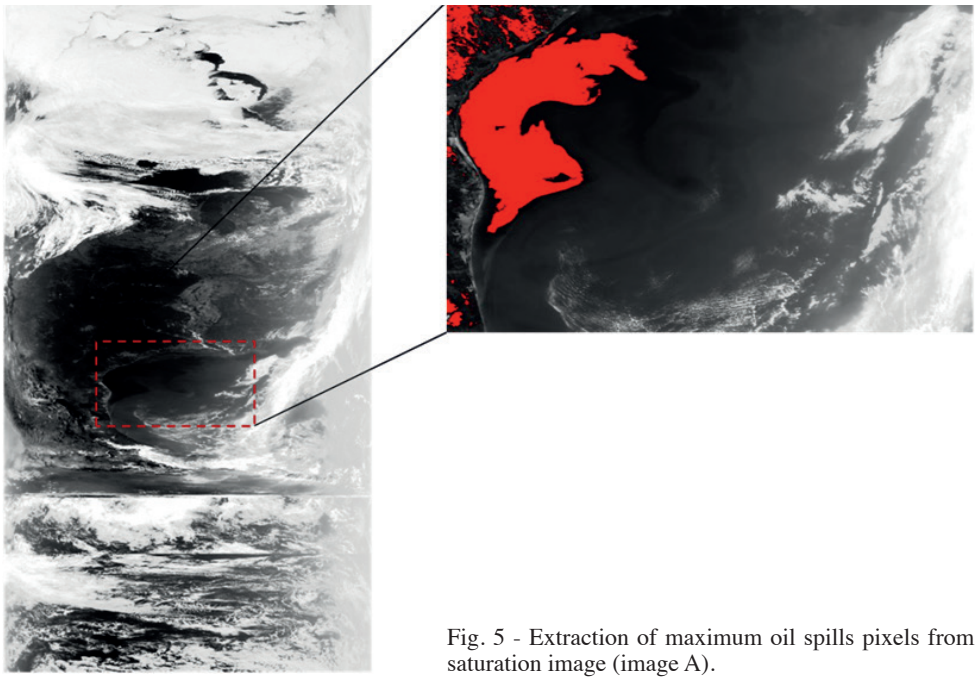

Fig. 5 - Extraction of maximum oil spills pixels from saturation image (image A).

$$OSPRRi[\%] = \frac{|Vi\ max - Vios\ max| + |Vi\ min - Vios\ min}{Vi\ max + Vios\ max + Vi\ min + Vios\ min} \times 100 \quad (7)$$

for the intensity images and:

$$OSPRRs[\%] = \frac{|Vs\ max - Vsos\ max| + |Vs\ min - Vsos\ min}{Vs\ max + Vsos\ max + Vs\ min + Vsos\ min} \times 100 \quad (8)$$

for the saturation images. In the above equations $Vi\,max$ and $Vs\,max$ indicate respectively the maximum value of the intensity and the saturation in each image (from image A to image F), while $Vi\,min$ and $Vs\,min$ are respectively the minimum value of the intensity and the saturation in each image (from image A to image F).

Table 2 - List of images used.

Image	Date of acquisition	Start time of acquisition	Region	Coordinates
Image A	04/05/2010	20:29:16 UTC	Louisiana coast, Gulf of Mexico	3.13 N / 95.3 W
Image B	05/04/2005	04:19:04 UTC	Yellow Sea, NE China's Liaoning Province coast	41.8 N / 121.3 E
Image C	18/01/2003	16:46:09 UTC	Lake Maracaibo, Venezuela	16.5 N / 73.5 W
Image D	31/10/2007	09:50:06 UTC	Arabian Gulf	31.3 N / 50.3 E
Image E	31/07/2006	10:50:08 UTC	Lebanese coast	39.0 N / 32.0 E
Image F	26/12/2007	14:01:34 UTC	Yellow Sea, west sea coast of Taean, Korea	38.3 N / 131.1 E

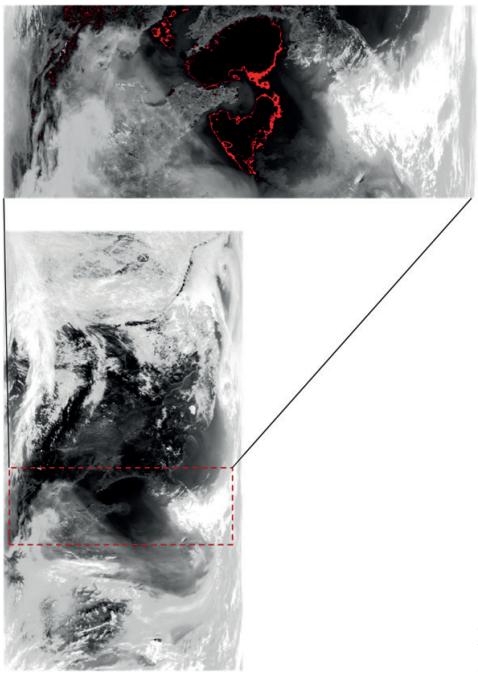

Fig. 6 - Extractions of the edge of oil spills pixels from the intensity image (image B).

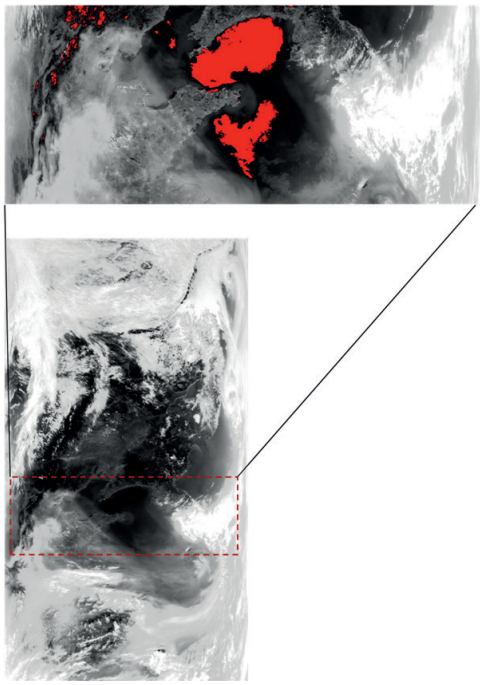

Fig. 7 - Extraction of maximum oil spills pixels from saturation image (image B).

On the other hand, *Vios max* and *Vsos max* are respectively the maximum value of the intensity and the saturation of oil spills pixels in each image (from image A to image F), *Vios min* and *Vsos min* are respectively the minimum value of the intensity and the saturation of oil spills pixels in each image (from image A to image H). The OSPRR ratio is applied to establish the efficiency of our method to localise the oil spills pixels for various environments.

Table 3 - Features of oil spills.

Image	Hue [°]	Saturation (S)	Intensity (I)
Image A	0-60	0-100	303-975
Oil slick coverage		45-60	407-424
OSPRR [%]		0	0
Image B	0-60	0-100	462-956
Oil slick coverage		46-61	406-424
OSPRR [%]		0.943	0.060
Image C	0-60	0-100	327-972
Oil slick coverage		45-59	407-425
OSPRR [%]		0.478	0.060
Image D	0-60	0-100	185-945
Oil slick coverage		44-61	406-425
OSPRR [%]		0.952	0.120
Image E	0-60	0-100	350-963
Oil slick coverage		43-62	404-422
OSPRR [%]		0-100	0.301
Image F	0-60	1.904	242-968
Oil slick coverage		45-62	408-426
OSPRR [%]		0.943	0.180

We can observe in Table 3 that the values of the OSPRRs [%] and the OSPRRi [%] are respectively in the interval [0.478, 1.904] and [0.060, 0.301]. In general, these results are very encouraging and promising, because the method can detect maximum pixels of oil slicks. The largest values are observed in image E, because of a small area of oil slicks in this scene of image (Fig. 8).

5. Conclusion

This paper presents an overview of one of the environmental phenomena: marine oil spills. SeaWiFS is an important tool in oil spill monitoring, because of the long field of view in the visible spectrum of the onboard sensor. In this paper, we proposed and applied an adapted method for monitoring and detection of oil slicks in SeaStar/SeaWiFS images. Each band is displayed in a monochromatic scale corresponding to its appropriate colour. When these are mixed, they produce the entire range of visible colours, creating an image that is fairly close to what the human eye would perceive.

A method derived from the RGB combination based on the computer vision techniques and RGB-to-HSI conversion is proposed. The colour masking technique is proposed to extract the maximum oil spill pixels from the SeaStar/SeaWiFS images. As a result, oil slicks pixels are obtained visually on the images intensity and saturation; then one looks at the values taken by intensity and saturation for potentially applying them to other images in routine.

We validated the proposed method by using other scenes of images with different dates and different regions. The obtained results show that the method can detect maximum pixels of oil

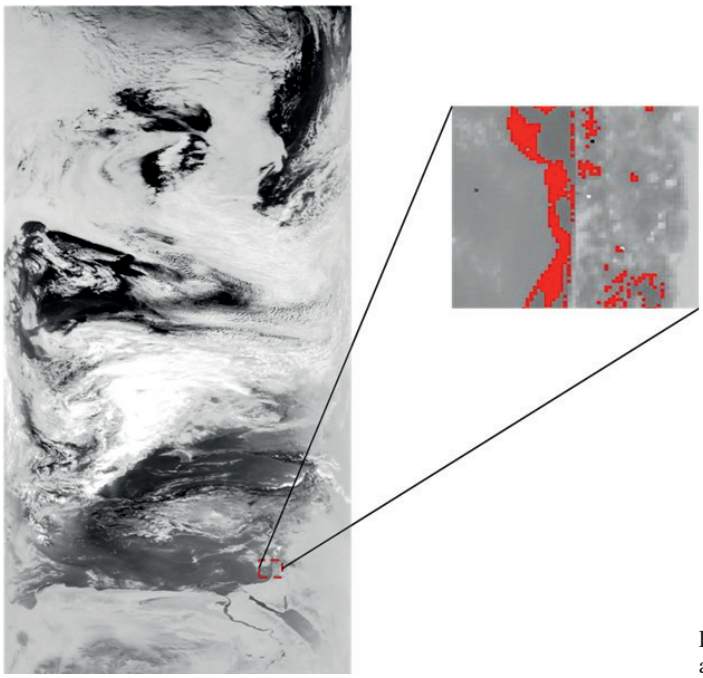

Fig. 8 - Image E: Lebanese coast with a small area of oil spills.

slicks. We establish that the method can be used to support the detection of oil spills, in spite of some limitations:

- small areas of oil spills cannot be depicted by the proposed method in some cases (operational oil spills, routine oil spills accident, etc.);
- the proposed method rest on human eyes examination, so we cannot analyse a large number of images in a short period of time;
- this method is used only in diurnal period of day;
- when the sky is cloudy, we cannot use this method.

Acknowledgements. The authors would like to thank the National Aeronautics and Space Administration (NASA) for the SeaWiFS scenes used for illustration purposes.

REFERENCES

Akar S., Süzen M.L. and Kaymakci N.; 2011: *Detection and object-based classification of offshore oil slicks using ENVISAT-ASAR images*. Environ. Monit. Assess., **183**, 409-423.

Brekke C. and Solberg A.H.S.; 2005: *Oil spill detection by satellite remote sensing*. Remote Sens. Environ., **95**, 1-13.

Bulgarelli B. and Djavidnia S.; 2012: *On MODIS retrieval of the marine environment*. IEEE Geosci. Remote Sens. Lett., **9**, 398-402.

Buono A., Nunziata F., Migliaccio M. and Li X.; 2016: *Mapping surface oil extent from the deepwater horizon oil spill using ASCAT backscatter*. IEEE Trans. Geosci. Remote Sens., **54**, 5862-5874.

Fingas M. and Brown C.; 1997: *Review of oil spill remote sensing*. Spill Sci. Tech. Bull., **4**, 199- 208.

Fingas M. and Brown C.; 2014: *Review of oil spill remote sensing*. Mar. Pollut. Bull., **83**, 9-23.

Friedman K.S., Pichel W.G., Clemente-Colon P. and Li X.; 2002: *GoMEx - an experimental GIS system for the Gulf of Mexico region using SAR and additional satellite and ancillary data*. In: Proc. IEEE Int. Geosci. Remote Sens. Symp., vol. 6, pp. 3343-3345.

Gambardella A., Giacinto G., Migliaccio M. and Montali A.; 2010: *One-class classification for oil spill detection*. Pattern Anal. Appl., **13**, 349-366.

Girard-Ardhuin F., Mercier G., Collard F. and Garello R.; 2005: *Operational oil-slick characterization by SAR imagery and synergistic data*. IEEE J. Oceanic Eng., **30**, 487-495.

Grégoire J.M., Cahoon D. and Stroppiana D.; 2002: *Marine Observation Satellites/Sensors*. In: Fundamentals of Remote Sensing, Canada Centre for Remote Sensing, Quebec, Canada, section 2.13, pp. 67-69.

Hassini A., Benabadji N. and Belbachir A.H.; 2005: *Reception of the APT weather satellite images*. Association for the Advancement of Modelling and Simulation Techniques in Enterprises (AMSE) J., Adv. B, **48**, 25-43.

Hassini A., Déjean S., Benabadji N., Hassini N. and Belbachir A.H.; 2008: *Forest fires smoke monitoring from sea-viewing wide field-of-view sensor images*. Opt. Appl. **38**, 737-754.

Horng W.B., Peng J.W. and Chen C.Y.; 2005: *A new image-based real-time flame detection method using color analysis*. IEEE International Conference on Networking, Sensing and Control, Tucson, AZ, USA, pp. 100-105.

Kaufman Y.J. and Remer L.A.; 1994: *Detection of forests using mid-IR reflectance: an application for aerosol studies*. IEEE Trans. Geosci. Remote Sens., **32**, 672-683.

Leblon B., García P.A.F., Oldford S., Maclean D.A. and Flannigan M.; 2007: *Using cumulative NOAAAVHRR spectral indices for estimating fire danger codes in northern boreal forests*. Int. J. Appl. Earth Obs., **9**, 335-342.

Leifer I., Luyendyk B. and Broderick K.; 2006: *Tracking an oil slick from multiple natural sources: Coal Oil Point, California*. Mar. Petrol. Geol., **23**, 621-630.

Lindsley R.D. and Long D.G.; 2012: *Mapping surface oil extent from the deepwater horizon oil spill using ASCAT Backscatter*. IEEE Trans. Geosci. Remote Sens., **50**, 2534-2541.

Linlin X., Li J. and Brenning A.; 2014: *A comparative study of different classification techniques for marine oil spill identification using RADARSAT-1 imagery*. Remote Sens. Environ., **141**, 14-23.

Lu Y., Li X., Tian Q. and Han W.; 2012: *An optical remote sensing model for estimating oil slick thickness based on two-beam interference theory*. Opt. Express, **20**, 24496-24504.

Lu Y., Tian Q., Wang X., Zheng G. and Li X.; 2013: *Determining oil slick thickness using hyperspectral remote sensing in the Bohai sea of China*. Int. J. Digital Earth, **6**, 76-93.

Migliaccio M., Nunziata F., Montuori A., Li X. and Pichel W.G.; 2011: *A multifrequency polarimetric SAR processing chain to observe oil fields in the Gulf of Mexico*. IEEE Trans. Geosci. Remote Sens., **49**, 4729-4737.

Migliaccio M., Nunziata F. and Buono A.; 2015: *A review on SAR polarimetry for sea oil slick observation*. Int. J. Remote Sens., **36**, 3243-3273.

Mihoub Z. and Hassini A.; 2014: *Monitoring and identification of marine oil spills using advanced synthetic aperture radar images*. Opt. Appl., XLIV, 433-449.

Munsell A.H.; 1969: *A grammar of color: a basic treatise on the color system*. Van Nostrand Reinhold Co., New York, NY, USA, 96 pp.

O'Brein G.W., Lawrence G.M., Williams A.K., Glenn K., Barrett A.G., Lech M., Edwards D.S., Cowley R., Boreham C.J. and Summons R.E.; 2005: *Yampi Shelf, Browse Basin, north-west Shelf, Australia: a test-bed for constraining hydrocarbon migration and seepage rates using combinations of 2D and 3D seismic data and multiple independent remote sensing technologies*. Mar. Petrol. Geol., **22**, 517-549.

Pisano A.; 2011; *Development of oil spill detection techniques for satellite optical sensors and their application to monitor oil spill discharge in the Mediterranean Sea*. Ph.D. Thesis in Environment Sciences, Department of Control and Management of Natural Resources, XXIII Ciclo, University of Bologna, Italy, 146 pp., doi: 10.6092/unibo/amsdottorato/3520.

Solberg A.H.S., Storvik G., Solberg R. and Volden E.; 1999: *Automatic detection of oil spills in ERS SAR images*. IEEE Trans. Geosci. Remote Sens., **37**, 1916-1924.

Taylor S.; 1992: *0.45 to 1.1 lm spectra of prudhoe crude oil and of beach materials in prince william sound, Alaska*. CRREL Special, Report No. 92-5.

Uchiyama T. and Arbib M.A.; 1994: *Color image segmentation using competitive learning*. IEEE Trans. Patt. Anal. Mach. Intell., vol. 16, pp. 1197-1206, doi: 10.1109/34.387488.

Williams A. and Lawrence G.; 2002: *The role of satellite seep detection in exploring the South Atlantic's ultra deep water*. In: Schumacher D. and LeSchack L.A. (eds.), Surface Exploration Case Histories: Applications of Geochemistry, Magnetics and Remote Sensing, AAPG Studies in Geology, No. 48 and SEG Geophysical References Series, No. 11, pp. 327-344.

Yuan Y., Xiong W., Fang Y., Lan T. and Li D.; 2010: *Detection of oil spills on water by differential polarization FTIR spectrometry*. Guang Pu Xue Yu Guang Pu Fen Xi, **30**, 2129-2132.

Yuan Y., Fang Y., Cui F. and Li D.; 2011: *Research on preprocessing algorithm for differential polarization spectrum of oil spills on water*. GuangxueXuebao/Acta Opt. Sin., **31**, 1128001-1–1128001-7.

Corresponding author: Zakarya Mihoub
LRPI Laboratory, Institute of Health and Industrial Safety, University of Batna-2
53 Route de Constantine, Fésdis, Batna 05078, Algeria
Phone: +213 778 083191; e-mail: zakaryahse@gmail.com